Spatiotemporal Multiplier Networks for Video Action Recognition

Christoph Feichtenhofer [*]
Graz University of Technology
feichtenhofer@tugraz.at

Axel Pinz
Graz University of Technology
axel.pinz@tugraz.at

Richard P. Wildes
York University, Toronto
wildes@cse.yorku.ca

Abstract

This paper presents a general ConvNet architecture for video action recognition based on multiplicative interactions of spacetime features. Our model combines the appearance and motion pathways of a two-stream architecture by motion gating and is trained end-to-end. We theoretically motivate multiplicative gating functions for residual networks and empirically study their effect on classification accuracy. To capture long-term dependencies we inject identity mapping kernels for learning temporal relationships. Our architecture is fully convolutional in spacetime and able to evaluate a video in a single forward pass. Empirical investigation reveals that our model produces state-of-the-art results on two standard action recognition datasets.

1. Introduction

Extremely deep representations have recently been highly successful in numerous pattern recognition competitions. Residual Networks (ResNets) [11] provide a structural concept for easing the training of deep architectures by inserting skip-connections for direct propagation of gradients from the loss layer at the end of the network to early layers close to the input. Recently, spatiotemporal ResNets (ST-ResNets) [8] have been presented as a combination of two-stream networks [28] with ResNets. The resulting architecture nontrivially extended the performance of the original two-stream approach in application to action recognition on standard datasets.

While the ST-ResNet [8] yielded state-of-the-art performance in application to action recognition, it did not provide systematic justification for its design choices. Our current work reconsiders the combination of the two-stream and ResNet approaches in a more thorough fashion to increase the understanding of how these techniques interact,

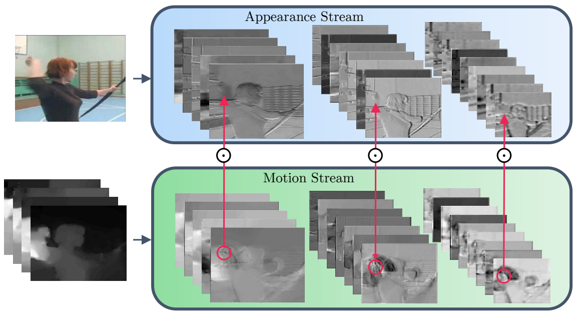

Figure 1. Motion gating at the feature level requires feature correspondence in the forward pass which is enforced through the gradient update of multiplicative interaction in the backward pass.

with a resulting novel architecture that produces a new state-of-the-art in action recognition.

More specifically, three main contributions are provided in this work. First, we show that a multiplicative motion gating of the appearance stream (Fig. 1) provides nontrivial performance boost over an additive formulation. We discuss the advantages of multiplicative interactions by the effect on the gradient in a residual network. We also verify their effectiveness in a series of ablation experiments where we systematically explore various alternatives for connecting the two streams, including bidirectional connections. Second, we discuss several approaches to generalizing the ST-ResNet architecture over long-term input. Here, we propose to inject temporal filters that are initialized as identity mapping kernels at the feature level. These temporal filters inject new layers in an existing model, while preserving the feature identity property of residual networks. This approach allows injection of new temporal aggregation filters even into the skip path of the network. We provide ablation studies for where to inject these mappings and how to initialize the temporal aggregation kernel. Third, based on what is learned from our investigation of fusing two-streams with residual connections and extending temporal support, we propose a *general* ConvNet architecture for action recognition in video. We provide details for how to learn a deep two-stream architecture that is fully convolutional in spacetime in an end-to-end fashion. We empirically show how multiplica-

[*]Christoph Feichtenhofer is a recipient of a DOC Fellowship of the Austrian Academy of Sciences at the Institute of Electrical Measurement and Measurement Signal Processing, Graz University of Technology.

tive motion gating between the streams and injected temporal aggregation filters can enhance performance substantially, leading to state-of-the-art performance on two popular action recognition datasets. Our code is available at https://github.com/feichtenhofer/multiplier-nets

2. Related work

Historically, research on video-based action recognition has mostly focused on crafting spatiotemporal features from optical flow-based motion information, *e.g*. Histograms Of Flow (HOF) [19], Motion Boundary Histograms (MBH) [3] and trajectories [37], or spatiotemporal oriented filtering *e.g*. HOG3D [16], Cuboids [5] and SOEs [4, 7].

More recently, researchers have focused on learning spatiotemporal features in an end-to-end fashion. Some work along these lines has concentrated on use of unsupervised learning [20, 33]. Other work makes use of a combination of hand-crafted and learned features [14]. In contrast, an alternative 3D spatiotemporal ConvNet, directly learned all of its filter kernels [35]. Interestingly, a work that compared a variety of approaches to extending 2D spatial ConvNets into time found little benefit of the temporal data [15].

Another relevant research direction for our concerns has addressed aggregation of temporal information over extended time periods. Here, a comparison of pooling approaches suggested good performance for temporal pooling of convolutional layers [25], as well as longer convolutions across time [36]. Perhaps the most straightforward approach comes from simple weighted averaging of video frames across time [2]. Greater complexity can be found in the various efforts that have incorporated LSTMs into their architectures to extend their temporal support (*e.g*. [23, 25, 27, 40]). Alternatively, RNNs have been applied for similar purposes [1, 22]. Other recent approaches rely on a Siamese architecture to abstract the temporal transformation of features across a video [39] or identify key volumes in the sequences [43].

The most closely related work to ours is the two-stream ConvNet architecture [28], which initially processes colour and optical flow information in parallel for subsequent late fusion of their separate classification scores. Extensions to that work that investigated convolutional fusion [9] and residual connections [8] are of particular relevance for the current work, as they serve as points of departure. In contrast to those previous efforts, the current work provides a more systematic investigation of the design space that leads to a novel architecture with improved performance.

3. Two-stream multiplier networks

3.1. Baseline architecture

We build our architecture on the two-stream approach [28], which separately trains two ConvNet streams: One stream exploits spatial appearance based on input of RGB image frames; the second exploits motion based on an input stack of $L = 10$ horizontal and vertical optical flow frames. Each stream performs video recognition on its own and prediction layer outputs are combined by late fusion for final classification. We found that training a ConvNet on both RGB and optical flow input is non-trivial, as such an architecture severely overfits to appearance information.

For each stream we use ResNets [11, 12] as the base network architecture. ResNets are fully convolutional architectures that, after an initial 7×7 filter, chain small spatial 3×3 convolutions with 1×1 dimensionality mapping filters [32] followed by batch normalization [13] and ReLU [17] non-linearities. The input is of size 224×224 and reduced five times in the network by stride 2 convolutions followed by global average pooling of the final 7×7 feature map. ResNets are equipped with additive skip connections to directly propagate signals to all layers of the network. The building blocks of the network are residual units defined as [11, 12]:

$$\mathbf{x}_{l+1} = f\left(\mathbf{x}_l + \mathcal{F}(\mathbf{x}_l; \mathcal{W}_l)\right), \tag{1}$$

where $\mathbf{x}_l$ and $\mathbf{x}_{l+1}$ are input and output of the l-th layer, $\mathcal{F}$ is a nonlinear residual mapping represented by convolutional filter weights $\mathcal{W}_l = \{\mathrm{W}_{l,k}|_{1\leq k\leq K}\}$ with $K \in \{2, 3\}$ and $f \equiv$ ReLU [12].

For both streams, we use the ResNet model [11] pretrained on the ImageNet CLSLOC dataset and replace the last layer according to the number of classes in the target dataset. Since the motion stream receives a stack of $2L = 20$ horizontal and vertical flow fields at the input, we replicate the first layer filters to fit that dimensionality.

3.2. Connecting the two streams

The original two-stream architecture only allowed the two processing paths to interact via late fusion of their respective softmax predictions [28]. That design did not support the learning of truly spatiotemporal features, which require the appearance and motion paths to interact earlier on during processing. This interaction, however, can be important for the discrimination of actions that have similar motion or appearance patterns and can only be disentangled by the combination of the two *e.g*. brushing teeth, applying a lipstick or shaving a beard. To address this limitation, we inject cross-stream residual connections. There are numerous ways in which such connections can be embodied. In our ablation studies we compare several variants (Fig. 2). We show that simple cross-residual connections between identical layers of the two streams leads to inferior classification performance compared to the (non-connected) two-stream baseline. We conjecture that the decrease in performance is due to the large change of the input distribution that the layers in one network stream undergo after injecting a fusion signal from the other stream.

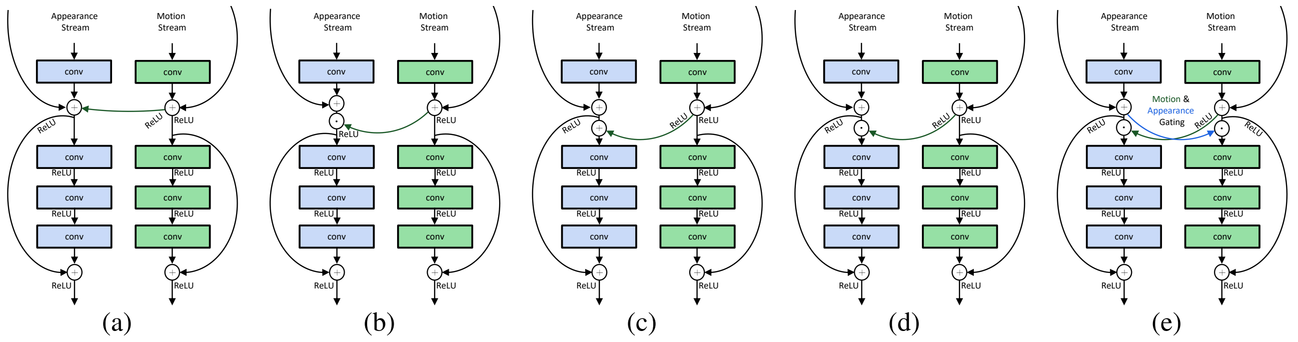

Figure 2. Different types of motion interactions between the two streams enables the learning of local spatiotemporal features. (a)-(d) show unidirectional connections from the motion into the appearance path and (e) illustrates bidirectional gating across streams.

3.2.1 Additive interaction

Recently, an approach has been presented that considers adding motion residuals to the appearance stream [8], as illustrated in Fig. 2(c) and formalized as

$$\hat{\mathbf{x}}^{\mathrm{a}}_{l+1} = f(\mathbf{x}^{\mathrm{a}}_l) + \mathcal{F}\Big(\mathbf{x}^{\mathrm{a}}_l + f(\mathbf{x}^{\mathrm{m}}_l), \mathcal{W}^{\mathrm{a}}_l\Big), \tag{2}$$

where $\mathbf{x}^{\mathrm{a}}_l$ and $\mathbf{x}^{\mathrm{m}}_l$ are the inputs of the l-th layers of the appearance and motion streams (resp.), while $\mathcal{W}^{\mathrm{a}}_l$ holds the weights of the l-th layer residual unit in the appearance stream. Correspondingly, the gradient on the loss function, $\mathcal{L}$, in the backward pass is given via the chain rule as

$$\begin{aligned}\frac{\partial \mathcal{L}}{\partial \mathbf{x}^{\mathrm{a}}_l} &= \frac{\partial \mathcal{L}}{\partial \hat{\mathbf{x}}^{\mathrm{a}}_{l+1}} \frac{\partial \hat{\mathbf{x}}^{\mathrm{a}}_{l+1}}{\partial \mathbf{x}^{\mathrm{a}}_l} \\ &= \frac{\partial \mathcal{L}}{\partial \hat{\mathbf{x}}^{\mathrm{a}}_{l+1}} \left(\frac{\partial f(\mathbf{x}^{\mathrm{a}}_l)}{\partial \mathbf{x}^{\mathrm{a}}_l} + \frac{\partial}{\partial \mathbf{x}^{\mathrm{a}}_l} \mathcal{F}\Big(\mathbf{x}^{\mathrm{a}}_l + f(\mathbf{x}^{\mathrm{m}}_l), \mathcal{W}^{\mathrm{a}}_l\Big) \right)\end{aligned} \tag{3}$$

for the appearance stream and similarly for the motion stream as

$$\frac{\partial \mathcal{L}}{\partial \mathbf{x}^{\mathrm{m}}_l} = \frac{\partial \mathcal{L}}{\partial \mathbf{x}^{\mathrm{m}}_{l+1}} \frac{\partial \mathbf{x}^{\mathrm{m}}_{l+1}}{\partial \mathbf{x}^{\mathrm{m}}_l} + \frac{\partial \mathcal{L}}{\partial \hat{\mathbf{x}}^{\mathrm{a}}_{l+1}} \frac{\partial}{\partial \mathbf{x}^{\mathrm{a}}_l} \mathcal{F}\Big(\mathbf{x}^{\mathrm{a}}_l + f(\mathbf{x}^{\mathrm{m}}_l), \mathcal{W}^{\mathrm{a}}_l\Big). \tag{4}$$

3.2.2 Multiplicative interaction

An interesting variation on the between stream interaction relates to multiplicative motion models (*e.g.* [24, 26, 34]) and treats the motion signal as gated modulation of the appearance features, illustrated in Fig. 2(d), and formalized as

$$\hat{\mathbf{x}}^{\mathrm{a}}_{l+1} = f(\mathbf{x}^{\mathrm{a}}_l) + \mathcal{F}\Big(\mathbf{x}^{\mathrm{a}}_l \odot f(\mathbf{x}^{\mathrm{m}}_l), \mathcal{W}_l\Big), \tag{5}$$

where $\odot$ corresponds to elementwise multiplication. A more detailed schematic is shown in Fig. 3. In this case, the gradient on the loss function, $\mathcal{L}$, during the backward pass can be expressed as

$$\begin{aligned}\frac{\partial \mathcal{L}}{\partial \mathbf{x}^{\mathrm{a}}_l} &= \frac{\partial \mathcal{L}}{\partial \hat{\mathbf{x}}^{\mathrm{a}}_{l+1}} \frac{\partial \hat{\mathbf{x}}^{\mathrm{a}}_{l+1}}{\partial \mathbf{x}^{\mathrm{a}}_l} \\ &= \frac{\partial \mathcal{L}}{\partial \hat{\mathbf{x}}^{\mathrm{a}}_{l+1}} \left(\frac{\partial f(\mathbf{x}^{\mathrm{a}}_l)}{\partial \mathbf{x}^{\mathrm{a}}_l} + \frac{\partial}{\partial \mathbf{x}^{\mathrm{a}}_l} \mathcal{F}\Big(\mathbf{x}^{\mathrm{a}}_l \odot f(\mathbf{x}^{\mathrm{m}}_l), \mathcal{W}^{\mathrm{a}}_l\Big) f(\mathbf{x}^{\mathrm{m}}_l) \right)\end{aligned} \tag{6}$$

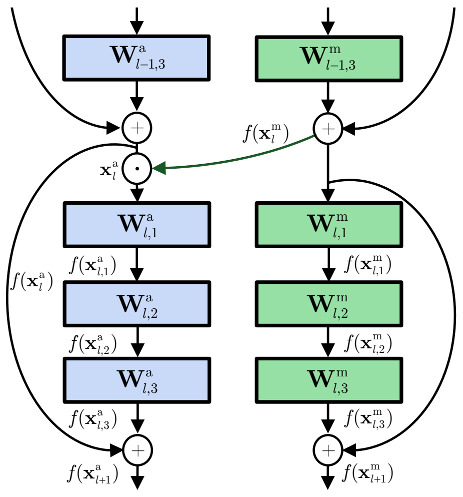
$\mathbf{W}^{\mathrm{a}}_{l-1,3}$
$\mathbf{W}^{\mathrm{m}}_{l-1,3}$
$f(\mathbf{x}^{\mathrm{m}}_l)$
$\mathbf{x}^{\mathrm{a}}_l$
$f(\mathbf{x}^{\mathrm{a}}_l)$
$\mathbf{W}^{\mathrm{a}}_{l,1}$ $\mathbf{W}^{\mathrm{m}}_{l,1}$
$f(\mathbf{x}^{\mathrm{a}}_{l,1})$ $f(\mathbf{x}^{\mathrm{m}}_{l,1})$
$\mathbf{W}^{\mathrm{a}}_{l,2}$ $\mathbf{W}^{\mathrm{m}}_{l,2}$
$f(\mathbf{x}^{\mathrm{a}}_{l,2})$ $f(\mathbf{x}^{\mathrm{m}}_{l,2})$
$\mathbf{W}^{\mathrm{a}}_{l,3}$ $\mathbf{W}^{\mathrm{m}}_{l,3}$
$f(\mathbf{x}^{\mathrm{a}}_{l,3})$ $f(\mathbf{x}^{\mathrm{m}}_{l,3})$
$f(\mathbf{x}^{\mathrm{a}}_{l+1})$ $f(\mathbf{x}^{\mathrm{m}}_{l+1})$

Figure 3. Illustration of multiplicative residual gating between the two streams (detailing Fig. 2(d)). During backpropagation the gradient is factored with the opposing stream's forward signal.

where the gradient flowing through the appearance stream's residual unit is modulated by the motion signal, $f(\mathbf{x}^{\mathrm{m}}_l)$. Mutually, the residual unit's gradient is modulated by the forwarded appearance signal $\mathbf{x}^{\mathrm{a}}_l$,

$$\frac{\partial \mathcal{L}}{\partial \mathbf{x}^{\mathrm{m}}_l} = \frac{\partial \mathcal{L}}{\partial \mathbf{x}^{\mathrm{m}}_{l+1}} \frac{\partial \mathbf{x}^{\mathrm{m}}_{l+1}}{\partial \mathbf{x}^{\mathrm{m}}_l} + \frac{\partial \mathcal{L}}{\partial \hat{\mathbf{x}}^{\mathrm{a}}_{l+1}} \frac{\partial}{\partial \mathbf{x}^{\mathrm{a}}_l} \mathcal{F}\Big(\mathbf{x}^{\mathrm{a}}_l \odot f(\mathbf{x}^{\mathrm{m}}_l), \mathcal{W}^{\mathrm{a}}_l\Big) \mathbf{x}^{\mathrm{a}}_l, \tag{7}$$

before addition to the motion stream gradient $\frac{\partial \mathcal{L}}{\partial \mathbf{x}^{\mathrm{m}}_{l+1}} \frac{\partial \mathbf{x}^{\mathrm{m}}_{l+1}}{\partial \mathbf{x}^{\mathrm{m}}_l}$. Thus, during backpropagation the current inputs of the motion $\mathbf{x}^{\mathrm{m}}_l$ and appearance $\mathbf{x}^{\mathrm{a}}_l$ streams are explicitly involved, acting as a gating mechanism on the gradient. This formulation makes the architecture particularly capable of learning spatiotemporal feature correspondences.

3.2.3 Discussion

Inclusion of the multiplicative interaction increases the order of the network fusion from first to second order [10]. Here, this multiplicative interaction between the two streams implies a much stronger signal change based on spatiotemporal feature correspondence compared to the additive interaction (2): In the former case, (5), the motion information directly scales the appearance information through the term $\mathbf{x}_l^{\mathrm{a}} \odot f(\mathbf{x}_l^{\mathrm{m}})$, rather than via a more subtle bias, $\mathbf{x}_l^{\mathrm{a}} + f(\mathbf{x}_l^{\mathrm{m}})$, as in the additive case, (2). During backpropagation, instead of the fusion gradient flowing through the appearance, (3), and motion, (4), streams being distributed uniformly due to additive forward interaction (2), it now is multiplicatively scaled by the opposing stream's current inputs, $f(\mathbf{x}_l^{\mathrm{m}})$ and $\mathbf{x}_l^{\mathrm{a}}$ in equations (6) and (7), respectively. This latter type of interaction allows the streams to more effectively interact during the learning process and corresponding spatiotemporal features thereby ultimately are captured (*cf.* similar discussion in the context of recurrent networks [41]).

Finally, rather than asymmetrically injecting the motion information into the appearance stream, bidirectional connections could be employed. Such processing could be realized for either additive or multiplicative interactions and is illustrated for the multiplicative case in Fig. 2(e). In empirical evaluation, we show that such interactions yield inferior performance to the asymmetric case of injecting motion into appearance. We conjecture that this result comes about because the spatial stream comes to dominate the motion stream during training.

3.3. Temporal filtering with feature identity

Beyond very limited means for interaction between its processing paths, the original two-stream network also employed only a small temporal window (10 frames) in making its predictions, which subsequently were averaged over the video [28]. In contrast, many real world actions required larger intervals of time to be defined unambiguously (*e.g.* consider a "lay-up" in basketball). Thus, the second way that we improve on the two-stream architecture is to provide it with greater temporal support (*cf.* [8, 9, 36] for previous work with similar motivations).

We employ 1D temporal convolutions combined with feature space transformations initialized as identity mappings to achieve our goal. 1D convolutions provide a learning-efficient way to capture temporal dependencies, *e.g.* with far less overhead than LSTMs. Initialization of the feature transformations as identity mappings is appropriate when injecting into deep architectures, as any significant change in the network path would distort the (pretrained) model and thereby remove most of its representational power. Furthermore, preserving the feature identity is essential to preserve the design principles of residual networks. The corresponding kernels can be injected at any point in the network since they do not impact the information flow at initialization; however, during training they can adapt their representation under the gradient flow.

Formally, we inject temporal convolutional layers into

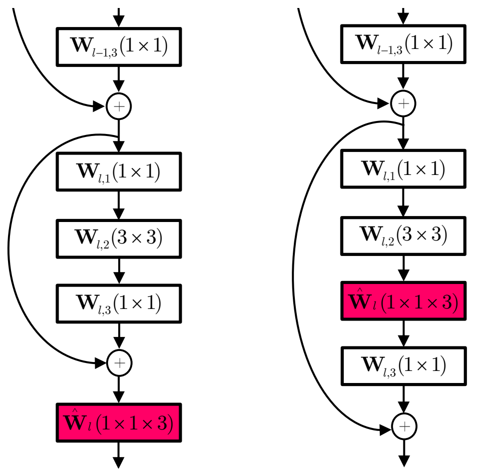
$\mathbf{W}_{l-1,3}(1\times1)$
$\mathbf{W}_{l,1}(1\times1)$
$\mathbf{W}_{l,2}(3\times3)$
$\mathbf{W}_{l,3}(1\times1)$
$\hat{\mathbf{W}}_l(1\times1\times3)$
$\mathbf{W}_{l-1,3}(1\times1)$
$\mathbf{W}_{l,1}(1\times1)$
$\mathbf{W}_{l,2}(3\times3)$
$\hat{\mathbf{W}}_l(1\times1\times3)$
$\mathbf{W}_{l,3}(1\times1)$

(a) † (b) ‡, §

Figure 4. Injection of identity mapping kernels as temporal filters, $\hat{W}_l$, into the skip path (a) or into the residual unit (b). Symbols †, ‡ and § are used in upcoming presentation to distinguish these cases.

the network that operate across C_l feature channels

$$\mathbf{x}_{l+1} = \mathbf{x}_l * \hat{W}_l + b_l, \tag{8}$$

where the biases b_l are initialized as $\mathbf{0}$ and $\hat{W}_l \in \mathbb{R}^{1\times1\times T\times C_l\times C_l}$ are temporal filters with weights initialized by stacking identity mappings between feature channels, $\mathbf{1} \in \mathbb{R}^{1\times1\times1\times C_l\times C_l}$, across $t = 1 \ldots T$. Specifically,

$$\hat{W}_l = \mathbf{1} \otimes \mathbf{f}, \tag{9}$$

where $\otimes$ denotes the tensor outer product and $\mathbf{f}$ is a 1D temporal filter of length T. Notably, eq. (9) initializes temporal kernels to perform identity transforms at feature level.

Since our kernels preserve the feature identity, we can place them after any layer in the network without affecting its representational ability (at initialization). During training, however, the newly added temporal conv layers affect the overall model. Here we distinguish two main variants, either inserting the layers in the shortcut path which directly affects all other layers in the network, or into the residual units which locally affects the surrounding blocks. These two variants for learning temporal relationships are illustrated in Fig. 4 and evaluated in our experiments (Sect. 5.2).

Recent ConvNet architectures [11, 31] are fully convolutional and use a global average pooling after the last conv layer. Generally global pooling is reasonable, since the exponentially expanding receptive field for deeper units typically spans the whole input, *e.g.* for the ResNet-50 the last convolutional layer has a theoretical receptive field of 483×483 pixels on the 224×224 sized input.

By design, our temporal convolutional layers, (8), provide broad temporal support, analogous to the broad spatial support that motivates global spatial pooling. Therefore, it is equally motivated to employ global temporal pooling.

Layers	conv1	pool1	conv2_x	conv3_x	conv4_x	conv5_x	pool5
			1×1, 64 3×3, 64 1×1, 256	1×1, 128 3×3, 128 1×1, 512	1×1, 256 3×3, 256 1×1, 1024	1×1, 512 3×3, 512 1×1, 2048	
			$\odot$	$\odot$	$\odot$	$\odot$	
Blocks	7×7, 64	3×3 max stride 2	1×1, 64 3×3, 64 ‡ 1×1, 256	1×1, 128 3×3, 128 ‡ 1×1, 512	1×1, 256 3×3, 256 ‡ 1×1, 1024	1×1, 512 3×3, 512 ‡, § 1×1, 2048	7×7 avg
			1×1, 64 3×3, 64 1×1, 256	1×1, 128 3×3, 128 1×1, 512 $\times N$	1×1, 256 3×3, 256 1×1, 1024 $\times M$	1×1, 512 3×3, 512 1×1, 2048	
			†	†	†	†	

Table 1. ResNet architecture used in our ConvNet streams. The layers are shown in the columns with brackets indicating residual units with skip connections. The filter dimensions are shown as $(W \times H, C)$ in brackets. $\odot$ denotes a multiplicative gate from the motion into the appearance stream, and the symbols ‡, § and † denote three alternatives for injecting the temporal filters. Notably for ‡ and § filters are injected only in the residual units (after a 3×3 convolution), whereas for † temporal filters also are injected into the shortcut path of the network. $N = 2$, $M = 4$ for a ResNet-50 and $N = 6$, $M = 32$ for a ResNet-152.

Here, our intial investigations showed that global max pooling over time led to superior results compared to average pooling, presumably because it allowed the network to capitalize on the most discriminative temporal sample. Therefore, given $\mathbf{x}(i,j,t,c)$ observed over $1 \leq t \leq T$ we pool according to

$$\mathbf{x}(i,j,c) = \max_{1 \leq t \leq T} \mathbf{x}(i,j,t,c). \quad (10)$$

During preliminary experiments, we also considered application of temporal max-pooling earlier in the network; however, it always produced inferior results to pooling after the last convolutional layer.

4. Architecture details

In our experiments we use 50 and 152 layer ResNets [11], pretrained on ImageNet. The building blocks of our 50-layer architecture are shown in Table 1 which reads from left to right, top to bottom. The operations at each block are convolution or pooling with dimensions $(W \times H, C)$, denoting width, height and number of feature channels, respectively. Each conv block is accompanied by batch normalization [13] and ReLU nonlinearities. The brackets indicate conv blocks that are grouped to residual units as outlined in equation (1). $\odot$ indicates the point of multiplicative motion gating into the appearance stream (Section 3.2.2) and the symbols ‡, § and † denote three variants of where to inject temporal convolutions (Sec. 3.3). In our ablation experiments we compare injecting temporal kernels into the skip path of every conv block (†), into a residual unit at every conv block (‡), or only into a residual unit at the last conv block (§); locally these variants are shown in Fig. 4.

4.1. Training procedure

We first separately train the two streams as described in [9, 28]. We start with a learning rate of 10^{-2} and lower it two times after the validation error saturates. Our motion network uses optical flow stacks with $L = 10$ frames and is trained with dropout of 0.8 after the final classification layer. Optical flow [42] is precomputed prior to training and stored as JPEG images (with displacement vectors > 20 pixels clipped). During training, we use the same augmentations as in [1, 39]; *i.e.* randomly cropping from the borders and centre of the flow stack and sampling the width and height of each crop randomly as $W, H \in \{256, 224, 192, 168\}$, followed by resizing to 224×224. We use a batch size of 128 by randomly sampling a single optical flow stack from a video. The effective batch size during each forward and backward pass is reduced to fit GPU memory constraints and the gradient update is applied after aggregating gradients for all 128 samples. Notably, for batch normalization [13] (which is applied at every forward/backward computation), the batch-size is smaller. We found this fact facilitates generalization performance of our model, because smaller batches increase the regularization effect of the noisy bias/variance estimates in batch normalization.

The appearance stream is trained analogously with a batch size of 256 RGB frames. Here, we apply a less aggressive scale augmentation than for the motion network: We randomly jitter the width and height of the 224×224 input frame by $\pm 25\%$ and also randomly crop it from a maximum of 25% distance from the image borders. The crop is rescaled to 224×224 and passed as input to the network.

The same rescaling and cropping technique is chosen to train our proposed model. Here, we sample 5 inputs from a video with random temporal stride between 5 and 35 frames (*i.e.* temporal jittering for the injected temporal conv-layers). The batch size is set to 128 videos where 5 temporal chunks are extracted from each one. Importantly, batch-normalization again uses a smaller batch size to fit GPU memory. The learning rate starts at 10^{-3} and is reduced by a factor of 10 after 20 epochs and again reduced by an order of magnitude after 10 epochs more.

case	into	Fig.	UCF101	HMDB51
direct $\oplus$	$\leftarrow$	Fig. 2(a)	24.78	54.85
direct $\odot$	$\leftarrow$	Fig. 2(b)	81.98	77.89
residual $\oplus$ Sect. 3.2.1	$\leftarrow$	Fig. 2(c)	9.38	41.89
residual $\odot$ Sect. 3.2.2	$\leftarrow$	Fig. 2(d)	<u>8.72</u>	<u>37.23</u>
residual $\oplus$	$\rightarrow$	Fig. 2(c)	16.76	49.54
residual $\odot$	$\rightarrow$	Fig. 2(d)	16.68	48.43
residual $\odot$	$\leftrightarrow$	Fig. 2(e)	15.15	48.56

Table 2. Classification error (%) on the first split of UCF101 and HMDB51 under different cross-stream connections.

4.2. Fully convolutional testing

We follow the evaluation procedure of the original two-stream work [28] by sampling 25 frames (and their horizontal flips). However, we apply fully convolutional testing both spatially (smallest side rescaled to 256) and temporally (the 25 frame-chunks) by classifying the video in a single forward pass. For inference, we average the predictions of the classification layers over all spatiotemporal locations. Despite our slightly better results with 10-crop testing, we prefer fully convolutional testing in spacetime as this method greatly increases inference speed (a video can be tested in $\approx$250ms on a single Nvidia Titan X GPU).

5. Experimental results

We validate our approach on two popular action recognition datasets: UCF101 [29], which consists of 13320 action videos in 101 categories and HMDB51 [18], consisting of 6766 videos in 51 categories. UCF101 provides videos with a fixed resolution of 320×240 showing large diversity in terms of action classes, variations in background, illumination, camera motion and viewpoint, as well as object appearance, scale and pose. HMDB51 [18] is a more challenging dateset with higher intra-class variations leading to larger errors during training and testing. For both datasets, we use the provided evaluation protocol and report the mean average accuracy over the three splits into training and test data. Our experiments are structured into four sections. First, we present ablation experiments on how to connect the two streams (Sect. 5.1). Second, we compare different strategies to inject identity mapping kernels for learning long temporal relationships (Sect. 5.2). Third, we investigate the impact of network depth (Sect. 5.3). Finally, we provide a comparison with the state-of-the-art (Sect. 5.4).

5.1. Analysis of Two-Stream connections

In Sect. 3.2 we discuss two specific ways of how to connect the two streams of our architecture. More generally, there are numerous ways how one could insert cross-stream connections. The goal here is to fuse the two networks (at a particular convolutional layer) such that channel responses at the same pixel position are put in correspondence. In previous work, different fusion functions have been discussed [9] where it has been shown that additive fusion performed better than maxout or concatenation of feature channels from the two paths. Additive fusion of ResNets has been used in [8], but was not compared to alternatives. In this section, we provide a more systematic analysis on cross-stream connections between the streams.

In Fig. 2 we illustrate the various possible flows of information through the network and in Table 2 we compare their performance as error on the first splits of UCF101 and HMDB51. Note that Fig. 2 only illustrates the connection structure for a single layer; the cross-stream connections are inserted at every conv block (as marked in Table 1). Table 2 lists the type of connection (direct or into residual units), the fusion function (additive $\oplus$ or multiplicative $\odot$), the direction (from the motion into the appearance stream $\leftarrow$, conversely $\rightarrow$ or bidirectional $\leftrightarrow$). Note that we do not show schematic figures for fusing from the appearance into the motion stream ($\rightarrow$), as these simply are horizontal reflections of the converse ones ($\leftarrow$).

We first focus on straightforward connection of the streams with an additive shortcut connection, Fig. 2(a), directly enabling forward and backward signal flow between the two paths. This strategy produces inferior results because it induces too large a change in the propagated signals, thereby disturbing the network's representation abilities. This overly aggressive change is induced in two ways: via the forwarded signal as it passes through the deep layers; via the backpropagated signal in all preceding layers that emit the fusion signal. Not surprisingly, the detriment is exacerbated when directly multiplying the shortcut paths of the two streams (Fig. 2(b) and second row of Table 2), because the change induced by multiplication is stronger than that from addition. More generally, injecting into the skip path breaks the identity shortcut of residual networks, thereby producing optimization difficulties [12] and significantly increased test error, as verified by our results.

Next, we compare the additive and multiplicative motion gating into the residual units, as presented in Sect. 3.2.1 and Sect. 3.2.2, resp. Injection of residuals from the motion stream has been employed previously in [8] and produces test errors of 9.38% and 41.89% on the first splits of UCF101 and HMDB51, resp. In comparison, merely changing the interaction to multiplicative gating reduces that error to 8.72% and 37.23%. The impact of multiplicative motion interaction is twofold: First, it directly gates corresponding appearance residual units; second, it modulates the gradient in the appearance and the motion stream by each other's current input features, thereby enforcing spatiotemporal feature correspondences.

As a further experiment, we invert the direction of the connection to fuse from the appearance into the motion stream. This variation again leads to inferior results, both for additive and multiplicative residual fusion. These results can be explained by a severe overfitting of the network to appearance information. In fact, when fusing from the appearance into the motion stream ($\rightarrow$), the training loss of the motion stream decreases much faster and ends up at a much lower value. The fast training error reduction is due to the networks' focus on appearance information, which is a much stronger modality for discriminating different training frames. This effect is not only the reason for fusing from the motion stream into the appearance stream, but also supports the design of having two loss layers at the end of the network. Finally, we performed an experiment for bidirectional connections Fig. 2(e), which also suffers under the effect of appearance dominating training.

Having verified the superior performance of multiplicative cross-stream residual connections, Fig. 2(d), compared to the alternatives considered, we build on that design for the remainder of the experiments, unless otherwise noted.

5.2. Experiments on temporal aggregation

This section provides experiments for our injection of temporal filter kernels that preserve feature identity at initialization. We explore several choices for injecting such kernels within the hierarchy of the network. Table 3 again reports the error on the first split of UCF101 and HMDB51, as we vary operations in three ways. First, we vary where the temporal kernel is injected into overall architecture (see Table 1, §, †, ‡). Second, we vary the initialization of the temporal filter kernels, which is the same for all feature channels, by setting them to perform either averaging, [⅓, ⅓, ⅓], or centering, [0, 1, 0], in time. Third, we vary whether or not max-pooling in time is employed. Significantly, during training the network inputs consist up to 11 chunks that are temporally strided in the range between 5 and 35 frames; thus, these kernels are able to learn long-term temporal relationships between the features.

The results show a clear benefit of adding temporal kernels that are able to learn longer temporal relationships. Compared to the multiplicative cross-stream gating baseline, benefit is had even if just a single temporal layer is injected into each stream (§). Further, when comparing the temporal initialization of the filters, the results indicate particular benefit of a centre initialization on HMDB51. We conjecture this is due to the temporal nature of HMDB51 in comparison to UCF101: HMDB51 exhibits a higher degree of inter-video diversity *e.g.* due to camera motion, whereas videos in UCF101 typically capture temporally consistent scenes.

Finally, we investigate the impact of temporal max pooling of features before the classification layer. We notice a further decrease in error rates to 6.00% and 30.98% on UCF101 and HMDB51, respectively. Here, the relative gains again can be explained by the temporal natures of the datasets. Notably, even if max-pooling is performed after the last convolutional layer, the network will use information from all frames that are within the span of the temporal kernels. Therefore, max-pooling conceptually is a meaningful operation, because it allows the network to set the focus on a particularly discriminating instance in time, even while considering long-term information captured by stacked temporal conv-layers. This property also holds during backpropagation. Here, max-pooling only backpropagates a single temporal gradient map, even while the stacked temporal convolutions expand their receptive field on the gradient inversely from the output to the input. Therefore, long-range information is also used for gradient updates.

case	temporal init.	pool time	UCF101	HMDB51
-	-	✗	8.72	37.23
§	[⅓, ⅓, ⅓]	✗	7.85	35.29
†	[⅓, ⅓, ⅓]	✗	7.72	35.96
‡	[⅓, ⅓, ⅓]	✗	<u>7.45</u>	35.94
†	[0, 1, 0]	✗	7.61	34.72
§	[0, 1, 0]	✗	7.74	34.90
‡	[0, 1, 0]	✗	7.79	<u>34.38</u>
†	[0, 1, 0]	✓	6.74	34.05
‡	[0, 1, 0]	✓	<u>6.00</u>	<u>30.98</u>

Table 3. Classification error (%) on the first split of UCF101 and HMDB51 under different temporal filtering layers. The symbols in the first column, §, †, ‡, denote where the new layers are placed within the overall architecture (see Table 1), temporal init indicates how the temporal filter taps are initialized (*i.e.* averaging or centre frame) and pool time indicates whether max-pooling in time is used during training and testing.

	UCF101		HMDB51	
Model	ResNet-50	ResNet-152	ResNet-50	ResNet-152
Appearance	82.3%	83.4%	48.9%	46.7%
Motion	87.0%	87.2%	55.8%	60.0%
Late Fusion	91.7%	91.8%	61.2%	63.8%

Table 4. Classification accuracy for 50 layer deep (ResNet-50), and extremely deep (ResNet-152) two-stream ConvNets on UCF101 and HMDB51. Using deeper networks boosts performance, except for the spatial network on HMDB51, which might be due to overfitting of the 152 layer model.

5.3. Going deeper

So far, all our ablation studies were conducted with a 50 layer deep ResNet model. We now switch from reporting classification error (that has been used in the ablation studies above) to accuracy, as this is the common measure in the action recognition literature. In Table 4 we report the accuracy for our two-stream baseline networks (no connections across streams or time) on all three splits the UCF101 and HMDB51 datasets. We train 50 and 152 layer models [11]. Classification is performed by averaging the prediction layer outputs from 25 uniformly sampled input video frames. Late fusion is implemented by averaging the prediction layer outputs. On HMDB51 we weight the temporal network scores by a factor of three before averaging. By comparing the performance we observe that the deeper appearance network degrades performance on HMDB51 (we were not able to ameliorate this effect with stronger regularization), while producing slightly better results on UCF101. In contrast, for the deeper motion network we see quite a sizable gain on HMDB51. These results motivate us to use a ResNet50 for the appearance and a ResNet-152 for the motion stream of our final architecture.

Method	UCF101	HMDB51
IDT [37]	86.4%	61.7%
Spatiotemporal ConvNet [15]	65.4%	-
Two-Stream ConvNet [28]	88.0%	59.4%
Long-term recurrent ConvNet [6]	82.9%	-
Composite LSTM Model [30]	84.3%	44.0
Two-Stream+LSTM [25]	88.6%	-
C3D [35]	85.2%	-
C3D + IDT [35]	90.4%	-
Dynamic Image Nets [2]	76.9%	42.8 %
Dynamic Image Nets [2] + IDT	89.1%	65.2%
Transformations[39]	92.4%	62.0%
Two-Stream Fusion[9]	92.5%	65.4%
Two-Stream Fusion[9] + IDT	93.5%	69.2%
Long-term ConvNets [36]	91.7%	64.8%
Long-term ConvNets [36] + IDT	92.7%	67.2%
VideoLSTM + IDT [22]	92.2%	64.9%
Hierarchical Attention Nets [40]	92.7%	64.3%
Key Volume Mining [43]	93.1%	63.3%
RNN-FV [21] + C3D [35] + IDT	94.1%	67.7%
Spatiotemporal ResNets [8]	93.4%	66.4%
TSN [38] + IDT flow	94.2%	69.0%
Spatiotemporal ResNets [8] + IDT	94.6%	70.3%
Ours	**94.2%**	**68.9%**
Ours + IDT	**94.9%**	**72.2%**

Table 5. Mean classification accuracy of the state-of-the-art on HMDB51 and UCF101.

5.4. Comparison with the state-of-the-art

In comparison to the current state-of-the-art in video action recognition (Table 5), we consistently improve classification accuracy when comparing to the spatiotemporal ResNet presented in [8] and other competitors.

As a final experiment, we are interested if there is still something to gain from a fusion with hand-crafted IDT features [37]. We simply average the $L2$ normalized SVM scores of Fisher vector encoded IDT features (*i.e.* HOG, HOF, MBH) with the prediction layer output of our ConvNet model. The resulting performance is shown in the final row of Table 5. We achieve 94.9% on UCF101 and 72.2% on HMDB51. These results indicate that the degree of complementary between hand-crafted representations and our end-to-end learned ConvNet approach is vanishing for UCF101, given the fact that other representations see much larger gains by fusion with IDT. Nevertheless, there is still a 3.7% increase on HMDB51, which we think is mainly due to dominant camera motion in HMDB51 that is explicitly compensated by IDT's warped flow.

An alternative approach that performs competitively to ours is TSN [38]. Notably, however, TSN relies on 2 more input modalities for training than does our approach: It pretrains the motion stream on TVL1 optical flow [42], IDT-flow [37] (termed warped flow in [38]) and difference images. This extra data yields much higher accuracy of their baseline two-stream net (*e.g.* 87.2% on UCF101's most difficult split1 in the motion stream where we have 84.9%). Thus, due to the implicit use of IDT during training, TSN [38] is not directly comparable to our results without IDT. Significantly, even given the advantage of using multiple input modalities for training a stronger baseline, the final TSN performance is merely equal to our results (without IDT).

6. Conclusion

This paper has addressed the challenging problem of learning multiscale spacetime representations for discriminative video recognition. We have presented a novel spatiotemporal architecture for video action recognition that builds on multiplicative interaction of appearance and motion features coupled with injected identity mapping kernels for learning long-term relationships. Our model is trained end-to-end and fully convolutional in spacetime to enable video classification in a single forward pass. In our systematic ablation studies we have underlined the importance of learning correspondences between highly abstract ConvNet features both spatially and temporally. Our results are in line with our derivations and suggest that our architecture should be applicable to related tasks such as localization and detection in video.

Acknowledgments. This work was partly supported by the Austrian Science Fund (FWF P27076) and NSERC.

References

[1] N. Ballas, L. Yao, C. Pal, and A. Courville. Delving deeper into convolutional networks for learning video representations. In *Proc. ICLR*, 2016. 2, 5

[2] H. Bilen, B. Fernando, E. Gavves, A. Vedaldi, and S. Gould. Dynamic image networks for action recognition. In *Proc. CVPR*, 2016. 2, 8

[3] N. Dalal, B. Triggs, and C. Schmid. Human detection using oriented histograms of flow and appearance. In *Proc. ECCV*, 2006. 2

[4] K. G. Derpanis, M. Sizintsev, K. Cannons, and R. P. Wildes. Action spotting and recognition based on a spatiotemporal orientation analysis. *IEEE PAMI*, 35(3):527–540, 2013. 2

[5] P. Dollár, V. Rabaud, G. Cottrell, and S. Belongie. Behavior recognition via sparse spatio-temporal features. In *Workshop on Visual Surveillance and Performance Evaluation of Tracking and Surveillance, in conjunction with the ICCV*, 2005. 2

[6] J. Donahue, L. A. Hendricks, S. Guadarrama, M. Rohrbach, S. Venugopalan, K. Saenko, and T. Darrell. Long-term recurrent convolutional networks for visual recognition and description. In *Proc. CVPR*, 2015. 8

[7] C. Feichtenhofer, A. Pinz, and R. Wildes. Dynamically encoded actions based on spacetime saliency. In *Proc. CVPR*, 2015. 2

[8] C. Feichtenhofer, A. Pinz, and R. Wildes. Spatiotemporal residual networks for video action recognition. In *NIPS*, 2016. 1, 2, 3, 4, 6, 8

[9] C. Feichtenhofer, A. Pinz, and A. Zisserman. Convolutional two-stream network fusion for video action recognition. In *Proc. CVPR*, 2016. 2, 4, 5, 6, 8

[10] M. Goudreau, C. Giles, S. Chakradhar, and D. Chen. First-order versus second-order single-layer recurrent neural networks. *IEEE Transactions on Neural Networks*, 5:511–513, 1994. 3

[11] K. He, X. Zhang, S. Ren, and J. Sun. Deep residual learning for image recognition. In *Proc. CVPR*, 2016. 1, 2, 4, 5, 8

[12] K. He, X. Zhang, S. Ren, and J. Sun. Identity mappings in deep residual networks. In *Proc. ECCV*, 2016. 2, 6

[13] S. Ioffe and C. Szegedy. Batch normalization: Accelerating deep network training by reducing internal covariate shift. In *Proc. ICML*, 2015. 2, 5

[14] S. Ji, W. Xu, M. Yang, and K. Yu. 3D convolutional neural networks for human action recognition. *IEEE PAMI*, 35(1):221–231, 2013. 2

[15] A. Karpathy, G. Toderici, S. Shetty, T. Leung, R. Sukthankar, and L. Fei-Fei. Large-scale video classification with convolutional neural networks. In *Proc. CVPR*, 2014. 2, 8

[16] A. Kläser, M. Marszałek, and C. Schmid. A spatio-temporal descriptor based on 3d-gradients. In *Proc. BMVC.*, 2008. 2

[17] A. Krizhevsky, I. Sutskever, and G. E. Hinton. ImageNet classification with deep convolutional neural networks. In *NIPS*, 2012. 2

[18] H. Kuehne, H. Jhuang, E. Garrote, T. Poggio, and T. Serre. HMDB: a large video database for human motion recognition. In *Proc. ICCV*, 2011. 6

[19] I. Laptev, M. Marszalek, C. Schmid, and B. Rozenfeld. Learning realistic human actions from movies. In *Proc. CVPR*, 2008. 2

[20] Q. V. Le, W. Y. Zou, S. Y. Yeung, and A. Y. Ng. Learning hierarchical invariant spatio-temporal features for action recognition with independent subspace analysis. In *Proc. CVPR*, 2011. 2

[21] G. Lev, G. Sadeh, B. Klein, and L. Wolf. RNN Fisher vectors for action recognition and image annotation. In *Proc. ECCV*, 2016. 8

[22] Z. Li, E. Gavves, M. Jain, and C. G. Snoek. VideoLSTM convolves, attends and flows for action recognition. *arXiv preprint arXiv:1607.01794*, 2016. 2, 8

[23] B. Mahasseni and S. Todorovic. Regularizing long short term memory with 3D human-skeleton sequences for action recognition. In *Proc. CVPR*, 2016. 2

[24] R. Memisevic and G. E. Hinton. Learning to represent spatial transformations with factored higher-order boltzmann machines. *Neural Computation*, 22(6):1473–1492, 2010. 3

[25] J. Y.-H. Ng, M. Hausknecht, S. Vijayanarasimhan, O. Vinyals, R. Monga, and G. Toderici. Beyond short snippets: Deep networks for video classification. In *Proc. CVPR*, 2015. 2, 8

[26] J. Oh, X. Guo, H. Lee, R. L. Lewis, and S. Singh. Action-conditional video prediction using deep networks in atari games. In *NIPS*, 2015. 3

[27] S. Sharma, R. Kiros, and R. Salakhutdinov. Action recognition using visual attention. In *NIPS workshop on Time Series*. 2015. 2

[28] K. Simonyan and A. Zisserman. Two-stream convolutional networks for action recognition in videos. In *NIPS*, 2014. 1, 2, 4, 5, 6, 8

[29] K. Soomro, A. R. Zamir, and M. Shah. UCF101: A dataset of 101 human actions calsses from videos in the wild. Technical Report CRCV-TR-12-01, 2012. 6

[30] N. Srivastava, E. Mansimov, and R. Salakhutdinov. Unsupervised learning of video representations using LSTMs. In *Proc. ICML*, 2015. 8

[31] C. Szegedy, W. Liu, Y. Jia, P. Sermanet, S. Reed, D. Anguelov, D. Erhan, V. Vanhoucke, and A. Rabinovich. Going deeper with convolutions. In *Proc. CVPR*, 2015. 4

[32] C. Szegedy, V. Vanhoucke, S. Ioffe, J. Shlens, and Z. Wojna. Rethinking the inception architecture for computer vision. *arXiv preprint arXiv:1512.00567*, 2015. 2

[33] G. W. Taylor, R. Fergus, Y. LeCun, and C. Bregler. Convolutional learning of spatio-temporal features. In *Proc. ECCV*, 2010. 2

[34] G. W. Taylor and G. E. Hinton. Factored conditional restricted boltzmann machines for modeling motion style. In *Proc. ICML*, 2009. 3

[35] D. Tran, L. Bourdev, R. Fergus, L. Torresani, and M. Paluri. Learning spatiotemporal features with 3D convolutional networks. In *Proc. ICCV*, 2015. 2, 8

[36] G. Varol, I. Laptev, and C. Schmid. Long-term temporal convolutions for action recognition. *arXiv:1604.04494*, 2016. 2, 4, 8

[37] H. Wang and C. Schmid. Action recognition with improved trajectories. In *Proc. ICCV*, 2013. 2, 8

[38] L. Wang, Y. Xiong, Z. Wang, Y. Qiao, D. Lin, X. Tang, and L. Val Gool. Temporal segment networks: Towards good practices for deep action recognition. In *ECCV*, 2016. 8

[39] X. Wang, A. Farhadi, and A. Gupta. Actions ~ transformations. In *Proc. CVPR*, 2016. 2, 5, 8

[40] Y. Wang, S. Wang, J. Tang, N. O'Hare, Y. Chang, and B. Li. Hierarchical attention network for action recognition in videos. *arXiv preprint arXiv:1607.06416*, 2016. 2, 8

[41] Y. Wu, S. Zhang, Y. Zhang, Y. Bengio, and R. Salakhutdinov. On multiplicative integration with recurrent neural networks. In *NIPS*, 2016. 4

[42] C. Zach, T. Pock, and H. Bischof. A duality based approach for realtime TV-L1 optical flow. In *Proc. DAGM*, pages 214–223, 2007. 5, 8

[43] W. Zhu, J. Hu, G. Sun, X. Cao, and Y. Qiao. A key volume mining deep framework for action recognition. In *Proc. CVPR*, 2016. 2, 8